Monthly Notices
of the
ROYAL ASTRONOMICAL SOCIETY

MNRAS **440,** 134–142 (2014)
Advance Access publication 2014 March 7

doi:10.1093/mnras/stu208

Evolution of extinction curves in galaxies

Ryosuke S. Asano,[1]★† Tsutomu T. Takeuchi,[1] Hiroyuki Hirashita[2] and Takaya Nozawa[3]

[1]*Department of Particle and Astrophysical Science, Nagoya University, Furo-cho, Chikusa-ku, Nagoya 464-8602, Japan*
[2]*Institute of Astronomy and Astrophysics, Academia Sinica, PO Box 23-141, Taipei 10617, Taiwan*
[3]*Kavli Institute for the Physics and Mathematics of the Universe (WPI), University of Tokyo, Kashiwa, Chiba 277-8583, Japan*

Accepted 2014 January 27. Received 2014 January 25; in original form 2013 November 25

ABSTRACT

We investigate the evolution of extinction curves in galaxies based on our evolution model of grain-size distribution. In this model, we considered various processes: dust formation by Type II supernovae and asymptotic giant branch stars, dust destruction by supernova shocks in the interstellar medium, metal accretion onto the surface of grains (referred to as grain growth), shattering and coagulation. We find that the extinction curve is flat in the earliest stage of galaxy evolution. As the galaxy is enriched with dust, shattering becomes effective, producing a large abundance of small grains ($a \lesssim 0.01\,\mu$m). Then, grain growth becomes effective at small grain radii, leading to the formation of a bump at $a \sim 10^{-3}$–$10^{-2}\,\mu$m on the grain-size distribution. Consequently, the extinction curve at ultraviolet (UV) wavelengths becomes steep, and a bump at $1/\lambda \sim 4.5\ \mu\mathrm{m}^{-1}$ (where λ is the wavelength) on the extinction curve becomes prominent. Once coagulation becomes effective, the extinction curves become flatter, but the UV extinction remains overproduced when compared with the Milky Way extinction curve. This discrepancy can be resolved by introducing a stronger contribution of coagulation. Consequently, the interplay between shattering and coagulation could be important in reproducing the Milky Way extinction curve.

Key words: ISM: clouds – dust, extinction – galaxies: evolution – galaxies: general – galaxies: ISM – stars: formation.

1 INTRODUCTION

Dust grains are one of the fundamental ingredients necessary for an understanding of the formation and evolution of galaxies. The surfaces of dust grains are the main sites for the formation of hydrogen molecules (e.g. Cazaux & Tielens 2004), which act as an effective coolant in low-metallicity conditions (e.g. Hirashita & Ferrara 2002; Cazaux & Spaans 2009). Dust is also an important coolant in star formation, inducing fragmentation into low-mass stars (Omukai et al. 2005; Schneider et al. 2006). Thus, dust grains are strongly related to star formation in galaxies. Furthermore, dust grains govern the scattering and absorption (i.e. extinction) of stellar light, in particular at short wavelengths such as the ultraviolet (UV), and re-emit in the infrared (IR). Consequently, dust grains significantly affect the spectral energy distribution (SED) of galaxies (e.g. Takagi, Vansevičius & Arimoto 2003).

The extinction curve, which represents the wavelength dependence of dust extinction, is used to relate the intrinsic stellar SED to the observed SED affected by dust extinction. Thus, the extinction curve is the fundamental tool for interpreting the observational SEDs of galaxies. Because the extinction curve depends strongly on the physical and optical properties of dust grains [grain size, dust components, etc.; see, for example, Mathis, Rumpl & Nordsieck 1977 (hereafter MRN); Weingartner & Draine 2001; Nozawa & Fukugita 2013], it is important to understand these properties.

The mean extinction curve of the Milky Way (hereafter the MW extinction curve) is observationally well investigated (e.g. Fitzpatrick & Massa 2007), and is widely adopted as a template extinction curve (e.g. Buat et al. 1999; Matsuoka et al. 2005; Kobayashi, Inoue & Inoue 2013; Krühler et al. 2013). The MW extinction curve has a bump at 2175 Å, which is thought to be generated by small carbonaceous grains and/or polycyclic aromatic hydrocarbons (PAHs; e.g. Barbaro et al. 2001; Draine 2009a), and shows a steep rise to the far-UV wavelength (called the UV slope). By fitting the MW extinction curve, MRN derived the grain-size distribution in the Milky Way, $f(a)\mathrm{d}a \propto a^{-3.5}\mathrm{d}a$, with $a = 0.005$–$0.25\,\mu$m, where a is the grain radius and $f(a)\mathrm{d}a$ is the number density of grains in the size interval $[a, a + \mathrm{d}a]$. However, Weingartner & Draine (2001) performed a detailed fit to the MW extinction curve, finding that the size distributions of carbonaceous and silicate dust grains are quite different from each other, contra MRN. The extinction curves depend on the line of sight, and Cardelli, Clayton & Mathis (1989) suggested that the variation of extinction curves can be described by adopting the parameter $R_V \equiv A_V/E(B-V)$, where A_V is the

★E-mail: asano.ryosuke@g.mbox.nagoya-u.ac.jp
† Fellow of the Japan Society for the Promotion of Science (JSPS).

magnitude of the extinction in the V band, and $E(B-V)$ is the reddening ($A_B - A_V$, where A_B is the extinction in the B band). Recently, Nozawa & Fukugita (2013) investigated the possible variety of dust properties based on the diversity of extinction curves observed in the Milky Way. They found that the power-law index and maximum radius of the grain-size distribution are tightly constrained to be -3.5 ± 0.2 and 0.25 ± 0.05 μm, respectively. Pei (1992) extended the graphite–silicate grain model that can fit the MW extinction curve (MRN) to the Large and Small Magellanic Clouds (LMC and SMC), and found that the extinction curves in these galaxies can be fitted with the MRN grain-size distribution by adjusting only the relative contribution of graphite and silicate.

Many studies have shown that high-z galaxies have different extinction curves from nearby galaxies (e.g. Maiolino et al. 2004; Liang & Li 2009; Gallerani et al. 2010; Hjorth et al. 2013). The extinction curve of the quasar SDSS104845.05+463718.3 (hereafter SDSS1048+4637) at redshift $z = 6.2$ has no 2175-Å bump, and is relatively flat at $\lambda \gtrsim 1700$ Å , rising towards shorter wavelengths at $\lambda \lesssim 1700$ Å. Maiolino et al. (2004), by using the model in Todini & Ferrara (2001), showed that the extinction curve is consistent with the dust formation in Type II supernovae (SNe II). Because of their short lifetimes (typically 10^{6-7} yr), SNe II are thought to be the origin of dust in the high-z Universe. On the other hand, because of the long lifetimes of progenitors, asymptotic giant branch (AGB) stars can be dominant sources of dust in galaxies at age $t > 1$ Gyr (but see Valiante et al. 2009). Furthermore, Hirashita et al. (2010) examined the extinction curves in starburst galaxies taking into account not only dust grains produced by SNe II but also the effect of shattering (grain–grain collision) in the warm ionized medium (WIM). They showed that the shattering can lead to the steepness of the extinction curve at UV wavelengths, and indicated that shattering may occur effectively in SDSS1048+4637. Liang & Li (2009) showed that the extinction curves of high-z gamma-ray bursts (GRBs) are different from those of the Milky Way and LMC. Among them, one at $z = 6.3$ appears to have the 2175-Å feature, indicating a difference from SDSS1048+4637. In order to reveal the origin of the differences in the extinction curves among galaxies in the high- and the low-z Universe, it is necessary to clarify the processes that govern the evolution of dust grains in galaxies.

An MRN-like power-law grain-size distribution can be realized if the grains are processed by grain–grain collisions (shattering and coagulation; e.g. Tanaka, Inaba & Nakazawa 1996; Kobayashi et al. 2010). Thus, it is probable that grain–grain collisions are an important process in the Milky Way and perhaps in nearby galaxies in general. In addition, if the metallicity in galaxies is larger than a certain value, the accretion of gas-phase metals onto the surface of pre-existing grains (referred to as 'grain growth' in this paper) occurs effectively (Inoue 2011; Asano et al. 2013a). Because grain growth has the potential to change the grain-size distribution [e.g. Hirashita & Kuo 2011; Asano et al. 2013b (hereafter A13)], the shape of extinction curves may change as a result of grain growth. In fact, Hirashita (2012) showed that the UV slope on extinction curves becomes steeper owing to grain growth if the grain-size distribution is initially similar to the MRN size distribution.

Various processes have different effects on different grain sizes. Grains ejected by SNe II into the interstellar medium (ISM) are relatively large ($a \gtrsim 0.01$ μm) owing to the destruction of small grains by the sputtering in reverse shocks (e.g. Bianchi & Schneider 2007; Nozawa et al. 2007). Grains produced in AGB stars may have typical radii ~ 0.1 μm (e.g. Winters et al. 1997; Ventura et al. 2012a,b; Di Criscienzo et al. 2013) and could be described by a log-normal distribution with a peak at $a \sim 0.1$ μm (Yasuda & Kozasa 2012). Furthermore, small grains ($a < 0.01$ μm) are efficiently destroyed by sputtering in interstellar shocks driven by SNe (Nozawa, Kozasa & Habe 2006). When grain growth occurs in the ISM, smaller grains grow more efficiently (e.g. Hirashita & Kuo 2011; A13) because the time-scale of grain growth is proportional to the volume-to-surface ratio of a dust grain. In the diffuse ISM, shattering can occur effectively if grains are dynamically coupled with magnetized interstellar turbulence (e.g. Yan, Lazarian & Draine 2004; Hirashita & Yan 2009); in particular, large grains ($a \gtrsim 0.1$ μm) acquire larger velocity dispersions than the shattering threshold velocities. Shattering also occurs in SN shocks (e.g. Jones, Tielens & Hollenbach 1996). In dense and cold regions, the coagulation of small grains can occur (e.g. Hirashita & Yan 2009; Ormel et al. 2009); consequently, the grain-size distribution shifts towards larger sizes (e.g. Hirashita & Li 2013). In summary, the above processes affecting grain-size distribution (referred to as 'dust processes' in this paper) are dependent on the metallicity, total dust amount, and grain-size distribution, and could be interrelated. Thus, it is necessary to construct a model that takes into account all dust processes in a unified framework.

There are a number of studies on the evolution of the grain-size distribution in galaxies (e.g. Liffman & Clayton 1989; O'Donnell & Mathis 1997; Hirashita et al. 2010; Yamasawa et al. 2011). However, they do not consider all the dust processes, in order to simplify the models. Recently, A13 discussed the evolution of the grain-size distribution, taking into account all the dust processes based on the chemical evolution of galaxies. A13 showed that the grain-size distribution drastically changes with galactic age because the dominant dust process changes (see Section 2). In view of the discussion in A13, it is expected that the extinction curve will also change with the galactic age owing to the change of the dominant dust processes. Therefore, in this paper, we examine the evolution of extinction curves in galaxies using the dust evolution model developed by A13, and check whether we can reproduce the MW extinction curve.

This paper is organized as follows. First, we briefly review the dust evolution model constructed by A13 and explain the theoretical treatment of the extinction curve in Section 2. In Section 3, we show the contributions of various dust processes to the extinction curve. We discuss how we can reproduce the MW extinction curve and the contribution of different grain species in Section 4. We present our conclusions in Section 5.

2 MODEL

In this section, we first review our dust evolution model for calculating the evolution of the grain-size distribution in a galaxy (A13). Then, we explain the method of calculating the extinction at wavelength λ, A_λ (in units of magnitude) based on the grain-size distribution calculated.

2.1 Dust evolution model

We briefly introduce the model constructed by A13 and summarize their results. A13 investigated the evolution of the grain-size distribution taking into account the dust formation by SNe II and AGB stars, dust destruction by SN shocks in the ISM, grain growth in the cold neutral medium (CNM), and grain–grain collisions (shattering and coagulation) in the warm neutral medium (WNM) and CNM. Grain growth in the WNM was not considered because grain growth is more efficient in dense, cold regions (e.g. Liffman & Clayton 1989; Draine 2009a). A13 considered the contribution of

the dust processes in the WNM and CNM by introducing the mass fractions of the WNM (∼6000 K, 0.3 cm^{-3}) and CNM (∼100 K, 30 cm^{-3}), $\eta_{\rm WNM}$ and $\eta_{\rm CNM}$, respectively. The sum of $\eta_{\rm WNM}$ and $\eta_{\rm CNM}$ was assumed to be unity in A13, as an equilibrium state of two thermally stable phases (WNM and CNM) is established in the ISM if we consider temperatures lower than 10^4 K (Wolfire et al. 2003). The grain velocities in the two ISM phases derived by Yan et al. (2004) were adopted to calculate shattering and coagulation.

We assume two dust species, graphite and silicate (Draine & Lee 1984), in the same way as in A13. Although A13 considered a variety of dust species (C, Si, SiO_2, SiC, Fe, FeS, Al_2O_3, MgO, $MgSiO_3$, Mg_2SiO_4 and Fe_2SiO_4; Nozawa et al. 2007; Zhukovska, Gail & Trieloff 2008) for stellar dust production, here carbonaceous dust and all the other dust species are categorized as graphite and silicate [we adopt astronomical silicate, $Mg_{1.1}Fe_{0.9}SiO_4$ (Draine & Lee 1984)], respectively, in order to avoid chemical complexity in grain growth, shattering, and coagulation. A13 examined the contribution of grain growth, shattering and coagulation for two dust species separately. While the complexity of dust species may affect the extinction curves (e.g. Nozawa & Fukugita 2013), the aim of this paper is not a detailed fit to a specific extinction curve but an investigation of the response of extinction curves to the evolution of grain-size distribution. Furthermore, it is thought that these two dust species are the main components of dust grains in the Milky Way (Draine & Lee 1984), and Sofia & Meyer (2001) suggested that the (Fe+Mg):Si ratio in dust grains is close to 2:1. Thus, the above grain composition is a reasonable approximation. Other possible dust species are discussed in Section 4. We assume that grains are spherical, and that shattering/coagulation occurs if the relative velocity of collisional grains is more/less than the threshold velocity (e.g. Yan et al. 2004; Hirashita & Yan 2009). The threshold velocity of shattering, $v_{\rm shat}$, is assumed to be 1.2 and 2.7 km s^{-1} for carbonaceous dust and silicate dust, respectively (Jones et al. 1996). For the threshold velocity of coagulation, we perform calculations as in Hirashita & Yan (2009), and the threshold velocity is about 10^{-3}–10^{-1} km s^{-1} depending on the grain size (Chokshi, Tielens & Hollenbach 1993). Note that if the radius of the shattered fragments is less than 3 Å, we remove the fragments, unlike in A13.

For the dust evolution model, A13 assumed that the total baryon mass (the sum of the stellar mass and the ISM mass in the galaxy) is constant (closed-box model), and formulated the star formation rate (SFR) by introducing the star formation time-scale, $\tau_{\rm SF}$: ${\rm SFR}(t) = M_{\rm ISM}(t)/\tau_{\rm SF}$, where $M_{\rm ISM}$ is the ISM mass and t is the galaxy age. Fig. 1 shows the evolution of the grain-size distribution (the sum of silicate and carbonaceous dust is shown) with all dust processes considered for $\tau_{\rm SF} = 5$ Gyr. We find that while the grain-size distribution is dominated by large grains ($a \gtrsim 0.1$ μm) produced by stars at <0.1 Gyr, as the galaxy evolution proceeds the grain-size distribution begins to be regulated by the processes in the ISM. In particular, once shattering occurs effectively, a large number of small grains ($a \lesssim 0.01$ μm) are produced by fragmentation owing to collisions between large grains. The effect of shattering is seen in the increase of small grains at 0.1–1 Gyr. Owing to the large number of small grains, grain growth occurs effectively because the surface-to-volume ratio of smaller grains is larger than that of larger grains. Consequently, the bump at $a \sim 0.01$ μm emerges at 1–10 Gyr. Smaller grains can acquire lower velocity dispersions because they are coupled with smaller-scale turbulence (e.g. Yan et al. 2004). Therefore, after the amount of small grains are increased, the coagulation occurs mainly by collisions between small grains whose velocity dispersions are smaller than the coagulation threshold. The shift of the bump position from 1 to 10 Gyr is a result of coagulation. For further details and parameter dependences of the grain-size distribution, see A13.

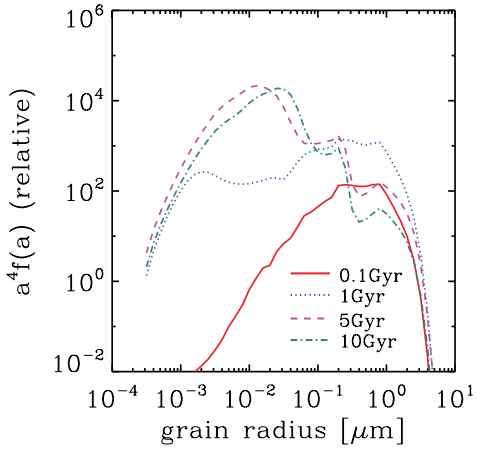

Figure 1. Example of the evolution of the grain-size distribution. Solid, dotted, dashed and dot–dashed lines represent the cases at $t = 0.1$, 1, 5, 10 Gyr, respectively, with $\tau_{\rm SF} = 5$ Gyr. The mass fractions, $\eta_{\rm WNM}$ and $\eta_{\rm CNM}$, are set to be 0.5.

2.2 Extinction curve

Extinction curves are powerful tools for examining the dust properties in galaxies. In order to analyse extinction curves, the optical constants for each dust species are necessary. In this paper, we adopt the optical constants derived by Draine & Lee (1984) to calculate the grain extinction cross-section normalized to the geometrical cross-section πa^2 as a function of wavelength and grain radius, $Q_{{\rm ext,\,X}}(\lambda, a)$, where the subscript X represents the grain species (X = carbonaceous dust or silicate dust), and λ is the wavelength.

The optical depth of dust species X at a given wavelength λ, $\tau_{{\rm X},\lambda}$, is defined as

$$\tau_{{\rm X},\lambda} = \int_0^\infty \pi a^2 C\, Q_{{\rm ext,X}}(\lambda, a)\, f_{\rm X}(a) {\rm d}a, \tag{1}$$

where C is a normalization constant and $f_{\rm X}(a)$ is defined so that $f_{\rm X}{\rm d}a$ is the number density of species X with radii in the range $[a, a + {\rm d}a]$. The extinction in units of magnitude is proportional to the optical depth, and is expressed as

$$A_{{\rm X},\lambda} = 1.086 \tau_{{\rm X},\lambda}, \tag{2}$$

where $A_{{\rm X},\lambda}$ is the extinction of dust species X in units of magnitude at wavelength λ. The total extinction in units of magnitude, A_λ, is expressed as

$$A_\lambda = \sum_{\rm X} A_{{\rm X},\lambda}. \tag{3}$$

In this work, we consider the extinction curve normalized to the V-band value, $A_\lambda / A_{\lambda_V}$, so C and the factor 1.086 cancel out.

3 RESULTS

In this section, we show the effects of each dust process on the extinction curve. We add the following processes one by one: the dust formation by SNe II and AGB stars, dust destruction by SN shocks in the ISM, grain growth in the ISM, shattering and coagulation in the ISM. The loss of dust by astration is always included, although it does not affect the shape of the extinction curve. We adopt a star

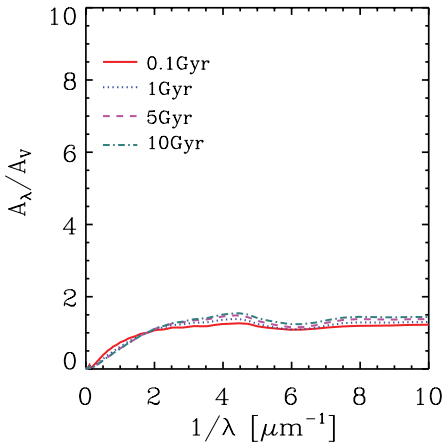

Figure 2. Evolution of extinction curves with dust formation by SNe II and AGB stars. Solid, dotted, dashed, and dot–dashed lines represent the cases at $t = 0.1$, 1, 5, 10 Gyr, respectively, with $\tau_{SF} = 5$ Gyr.

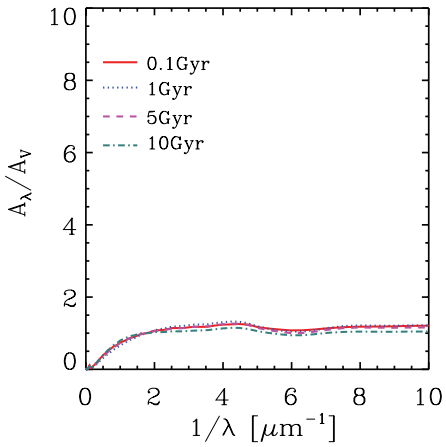

Figure 3. As Fig. 2, but including dust destruction by SN shocks in the ISM.

formation time-scale of $\tau_{SF} = 5$ Gyr, and mass fractions of the WNM and CNM of $\eta_{WNM} = \eta_{CNM} = 0.5$ unless otherwise stated.

3.1 Dust formation by SNe II and AGB stars

In Fig. 2, we show the evolution of extinction curves with dust formation by SNe II and AGB stars. From Fig. 2, it can be seen that the extinction curves are flat throughout galactic ages, and do not change significantly with time. This is because the size distribution of grains produced by SNe II and AGB stars is dominated by large grains ($a \gtrsim 0.1$ μm) (Nozawa et al. 2007; Yasuda & Kozasa 2012) and does not change appreciably with galactic age (fig. 1 of A13).

A13 showed that, although the size distribution of grains produced by SNe II depends on the hydrogen number density of the ISM surrounding the SNe II, n_{SN} (we adopt $n_{SN} = 1.0\,cm^{-3}$ in this paper), the tendency that the grain-size distribution is dominated by large grains is unchanged.

3.2 Dust destruction

In Fig. 3, we show the evolution of an extinction curve with dust destruction by SN shocks in the ISM in addition to the dust formation by stars. The time-scale on which the dust destruction affects the grain-size distribution in galaxies, τ_{SN}, is about $\tau_{SN} \sim 0.1\tau_{SF}$

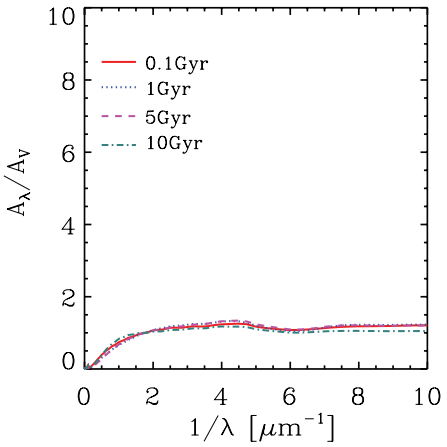

Figure 4. As Fig. 3, but including grain growth. We adopt $\eta_{CNM} = 0.5$.

(A13). Thus, we cannot observe the difference between the extinction curves with and without dust destruction at 0.1 Gyr (solid lines in Figs 2 and 3). The extinction curves with dust destruction are slightly flatter than those produced by stardust (see Fig. 2) at $t \gtrsim 1$Gyr. Because smaller grains are more easily destroyed by SN shocks (Nozawa et al. 2006; Yamasawa et al. 2011; A13), the extinction curves become flatter than in the case without dust destruction by SN shocks in the ISM (Fig. 2).

A13 examined the effect of dust destruction by SN shocks in the ISM for various n_{SN}, and showed that the effect is larger for larger n_{SN}. Thus, the extinction curve becomes flatter for larger n_{SN}.

3.3 Grain growth

Fig. 4 shows the evolution of extinction curves with dust formation by SNe II and AGB stars, dust destruction by SN shocks in the ISM, and grain growth in the CNM. We find that the extinction curves are almost the same as in Fig. 3. In this case, because the total surface area of grains is dominated by large grains with $a > 0.3$ μm (A13), the effect of grain growth is prominent at large sizes ($a \gtrsim 0.1$ μm). Because the grains are already large, grain growth just keeps the extinction curve flat.

3.4 Shattering

We now consider the evolution of an extinction curve with shattering in addition to all the dust processes considered in Section 3.3. From Fig. 5, we observe that the extinction curve is almost flat until galactic age $t \sim 1$ Gyr; at $t \lesssim 1$ Gyr, shattering is ineffective owing to the small dust abundance, and the grain-size distribution is similar to in the case without shattering (A13). A13 discussed the time-scale on which the grain-size distribution changes owing to the processes in the ISM (especially shattering), and obtained the time-scale $\tau_{shat} \sim 1(\tau_{SF}/\mathrm{Gyr})^{1/2}$ Gyr from a rough order-of-magnitude estimate (see their appendix B). Thus, there is only a small difference between the cases with and without shattering at $t < 1$ Gyr for $\tau_{SF} = 5$ Gyr. At $t = 5$ Gyr, the extinction curve drastically changes and starts to have a prominent bump at $1/\lambda \sim 4.5\ \mu m^{-1}$ (the so-called 2175-Å bump) and a steep slope towards shorter wavelengths. This is because the grain-size distribution changes considerably owing to the interplay between grain growth and shattering (A13). A13 showed that once shattering occurs effectively, the number of small grains increases with the decrease in the number of large grains. Thus, the total surface area of grains per grain mass becomes large, and grain growth occurs effectively, especially at small grain radii

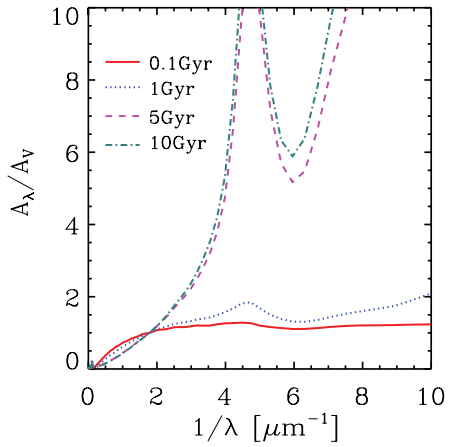

Figure 5. As Fig. 4, but including shattering. We adopt $\eta_{\rm WNM} = \eta_{\rm CNM} = 0.5$.

($\lesssim$0.01 μm), forming a bump at $a \sim 0.01$ μm in the grain-size distribution. Consequently, the 2175-Å bump and UV slope on the extinction curve become larger and steeper, respectively. In fact, Hirashita (2012) also showed that the 2175-Å bump and the UV slope are enhanced by grain growth. At $t = 10$ Gyr, although grain growth becomes ineffective owing to the large depletion of heavy elements (e.g. Asano et al. 2013a), the abundance of small grains still increases by shattering. Consequently, the 2175-Å bump and the UV slope become larger and steeper at 10 Gyr than at 5 Gyr.

3.5 Coagulation

In Fig. 6, we show the evolution of the extinction curve with all the dust processes considered in our model. We find that the extinction curves at $t = 0.1$ and 1 Gyr are flat, and that there is little difference between the extinction curves with and without coagulation (see Fig. 5). As mentioned in Section 2.1, because coagulation occurs when the relative velocity of colliding grains is less than $v_{\rm coag}$ [fiducial $v_{\rm coag} \sim 10^{-3}$–$10^{-1}$ km s^{-1}, depending on the grain size (Chokshi et al. 1993)], coagulation does not occur for large grains ($a \gtrsim 0.1$ μm) whose velocities are above the coagulation threshold. At $t = 5$ and 10 Gyr, the 2175-Å bump is smaller, and the UV slope is flatter than those in the case without coagulation (Fig. 5). A13 showed that the bump at $a \sim 0.01$ μm in the grain-size distribution shifts to larger sizes by coagulation, and finally moves to $a \sim 0.03$–0.05 μm at 10 Gyr. As the abundance of large grains is increased by coagulation, the bump at $1/\lambda \sim 4.5$ μm^{-1} and the UV slope become smaller and flatter, respectively.

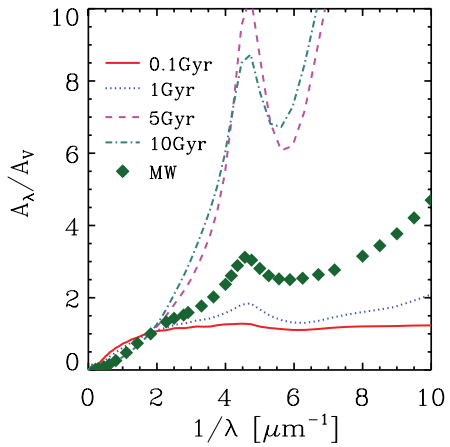

Figure 6. As Fig. 5, but including coagulation. Filled diamonds represent the extinction curve of the Milky Way (Whittet 2003).

For reference, we show the MW extinction curve taken from Whittet (2003) in Fig. 6. We find that our calculated extinction curve at the age of the Milky Way (∼10 Gyr) is steeper and has a larger 2175-Å bump than the observed extinction curve of the Milky Way. The main aim of this paper is not to reproduce the MW extinction curve precisely but to examine the trend of evolution of the extinction curve. Nevertheless, we will propose and examine some possibilities of reproducing the MW extinction curve by slightly modifying our model in Section 4.1.

3.6 Parameter dependence

So far, we have adopted the star formation time-scale $\tau_{\rm SF} = 5$ Gyr, and mass fractions of the WNM and CNM of $\eta_{\rm WNM} = \eta_{\rm CNM} = 0.5$ as a fiducial case. Here, we demonstrate how the extinction curve depends on these parameters.

In panels (a) and (b) of Fig. 7, we show the time evolution of the extinction curve in the cases of $\tau_{\rm SF} = 0.5$ and 50 Gyr, respectively, for $\eta_{\rm WNM} = \eta_{\rm CNM} = 0.5$. Focusing on (a), we find that the extinction curve at 1 Gyr is different from that in Fig. 6, where $\tau_{\rm SF} = 5$ Gyr is adopted. If $\tau_{\rm SF}$ is short, the total dust amount ejected by stars is large at younger galactic ages. This early increase in dust abundance shortens the time-scale on which shattering becomes effective according to $\tau_{\rm shat} \sim 1(\tau_{\rm SF}/{\rm Gyr})^{1/2}$ Gyr (A13; Section 3.4). Thus, shattering is already able to produce a large amount of small grains at <1 Gyr for $\tau_{\rm SF} = 0.5$ Gyr. Consequently, the extinction curve has the 2175-Å bump and steep UV slope at earlier phases of galaxy evolution. We also observe that the extinction curves at $t = 5$ and 10 Gyr are almost identical to each other. This means that the grain-size distribution does not change at these ages for $\tau_{\rm SF} = 0.5$ Gyr. Because the total dust amount decreases rapidly by astration in the case with the short star formation time-scale (e.g. Asano et al. 2013a), shattering and coagulation become inefficient at those ages. As a result, the shape of the grain-size distribution does not change significantly. On the other hand, Fig. 7(b) shows the result for $\tau_{\rm SF} = 50$ Gyr. We find that the 2175-Å bump continues to grow even after 5 Gyr. This is because the increase of the total dust amount is slower owing to the longer star formation time-scale than in (a). Indeed, $\tau_{\rm shat} \sim 7$ Gyr is consistent with the rapid increase of small grains at 5–10 Gyr (see also fig. 9 in A13). Thus, the time-scales of all dust processes we considered become long (e.g. A13), and the evolution of the extinction curve slows down.

Panels (c) and (d) of Fig. 7 show the cases with ($\eta_{\rm WNM}$, $\eta_{\rm CNM}$) = (0.1, 0.9) and (0.9, 0.1), respectively, for $\tau_{\rm SF} = 5$ Gyr. Because a large $\eta_{\rm CNM}$ is adopted in (c), the time-scale of coagulation is short. Consequently, the 2175-Å bump becomes small at earlier phases than in the case with a small $\eta_{\rm CNM}$. In (d), where a small $\eta_{\rm CNM}$ is adopted, the time-scale of grain growth is longer than that for (c). As mentioned in Section 3.4, the 2175-Å bump becomes prominent owing to grain growth. Thus, the 2175-Å bump becomes more prominent at later phases than in the case with a larger $\eta_{\rm CNM}$.

4 DISCUSSION

4.1 Reproducing the MW extinction curve

In the previous section, we examined the evolution of the extinction curve in galaxies taking into account various dust

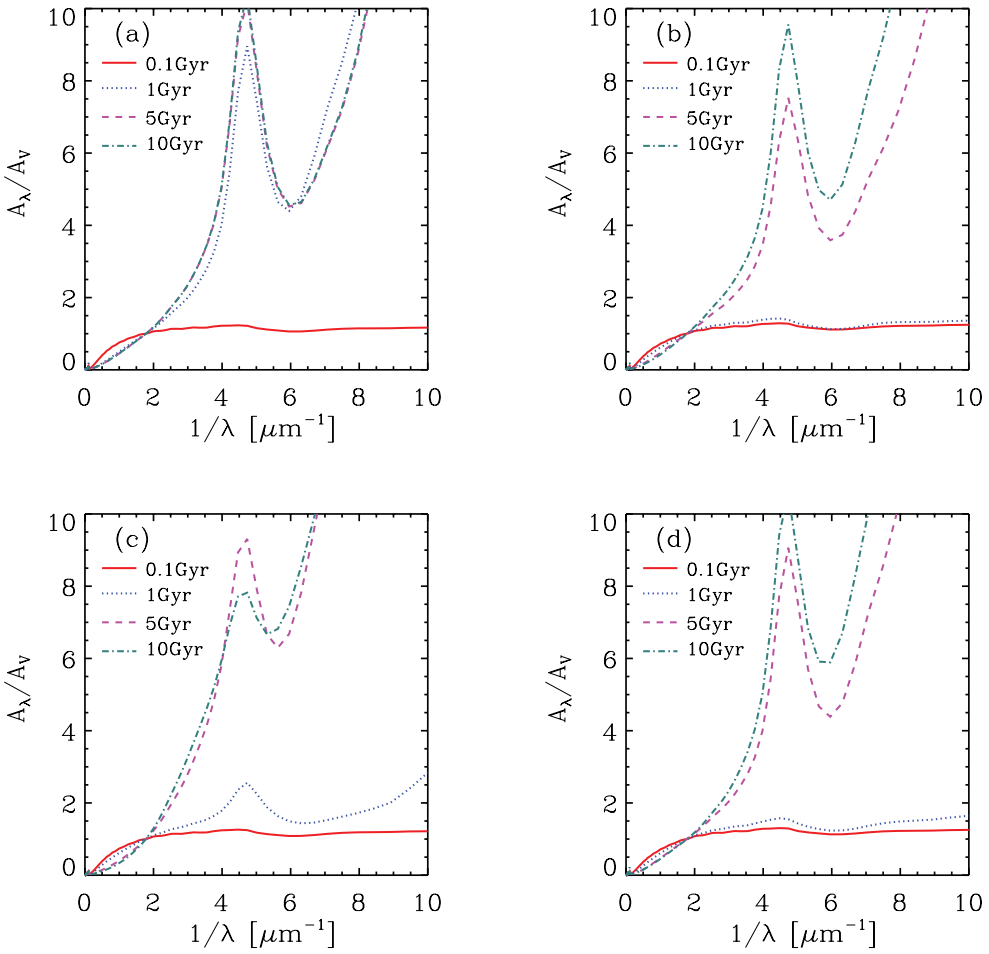

Figure 7. As Fig. 6, but with (a) $\tau_{SF} = 0.5$ Gyr and $\eta_{WNM} = \eta_{CNM} = 0.5$; (b) $\tau_{SF} = 50$ Gyr and $\eta_{WNM} = \eta_{CNM} = 0.5$; (c) $\tau_{SF} = 5$ Gyr, $\eta_{WNM} = 0.1$ and $\eta_{CNM} = 0.9$; and (d) $\tau_{SF} = 5$ Gyr, $\eta_{WNM} = 0.9$ and $\eta_{CNM} = 0.1$.

processes. We found that because stellar dust is biased to large grains ($a \gtrsim 0.1\,\mu$m), the extinction curve at the earliest stage of galaxy evolution is flat. After $t \sim \tau_{shat} \sim 1(\tau_{SF}/\mathrm{Gyr})^{1/2}$ Gyr, shattering and grain growth occur effectively, and the extinction curve becomes steeper and has a larger bump at $1/\lambda \sim 4.5\,\mu m^{-1}$ than in the case of the MW extinction curve. After coagulation becomes effective, the bump becomes small. However, compared with the MW extinction curve, the calculated extinction curves are too steep and have too large a bump. The reason for this is too abundant small grains, forming the bump at $a \sim 0.01\,\mu$m in the grain-size distribution (Fig. 1). Thus, it is crucial to weaken this bump in order to reproduce the MW extinction curve. As explained in Section 3.4, the bump in the grain-size distribution is formed by grain growth. This means that our models may have overestimated grain growth. Thus, as the first possibility of reproducing the MW extinction curve, we examine a model in which only grain growth is turned off. This is referred to as (i) the no grain growth model.

There is another way of weakening the bump in the grain-size distribution. In the current model, coagulation takes place only for grains with radii less than $\sim$0.05 μm, because large grains have larger velocities than the coagulation threshold (Section 3.5). However, if the grains can coagulate beyond 0.05 μm, the bump in the grain-size distribution could be smoothed out. There are some indications that the grains could coagulate beyond 0.05 μm: Ossenkopf (1993) argued that fluffy grains can be formed in dense regions by coagulation. Fluffiness enhances the cross-section in grain–grain collisions, raising the coagulation rate. Fluffy grains can also absorb collision energy, raising the coagulation threshold (e.g. Ormel et al. 2009). Enhancement of coagulation efficiency is also suggested by Hirashita & Li (2013) to explain μm-sized grains in dense molecular cloud cores. Thus, to investigate the possibility of strong coagulation, we examine a model with no coagulation threshold velocity. This model is referred to as (ii) the strong coagulation model.

Fig. 8 shows the extinction curves and the grain-size distributions for carbon and silicate dust at the galactic age of 10 Gyr for (i) the no grain growth model and (ii) the strong coagulation model. We adopt $\tau_{SF} = 5$ Gyr, $\eta_{WNM} = \eta_{CNM} = 0.5$. For comparison, we show the grain-size distribution using the same parameters as in Section 3.5 for a fiducial case. In both panels, we find that the MW extinction curve is better reproduced than for the cases considered in Section 3. For the no grain growth model (top panels), we observe that the calculated extinction curve is similar to that of the Milky Way, as the shape of the grain-size distribution is similar to the MRN distribution. This is because when grain growth is not considered, the bump produced at $a < 0.01\,\mu$m in the size distribution (see Fig. 1) cannot be formed. Consequently, the grain-size distribution approaches a power-law size distribution with a power index ~ -3.5 because shattering and coagulation are dominant processes in the formation of the grain-size distribution (e.g. Kobayashi et al. 2010). However, if we do not consider the contribution of grain growth to

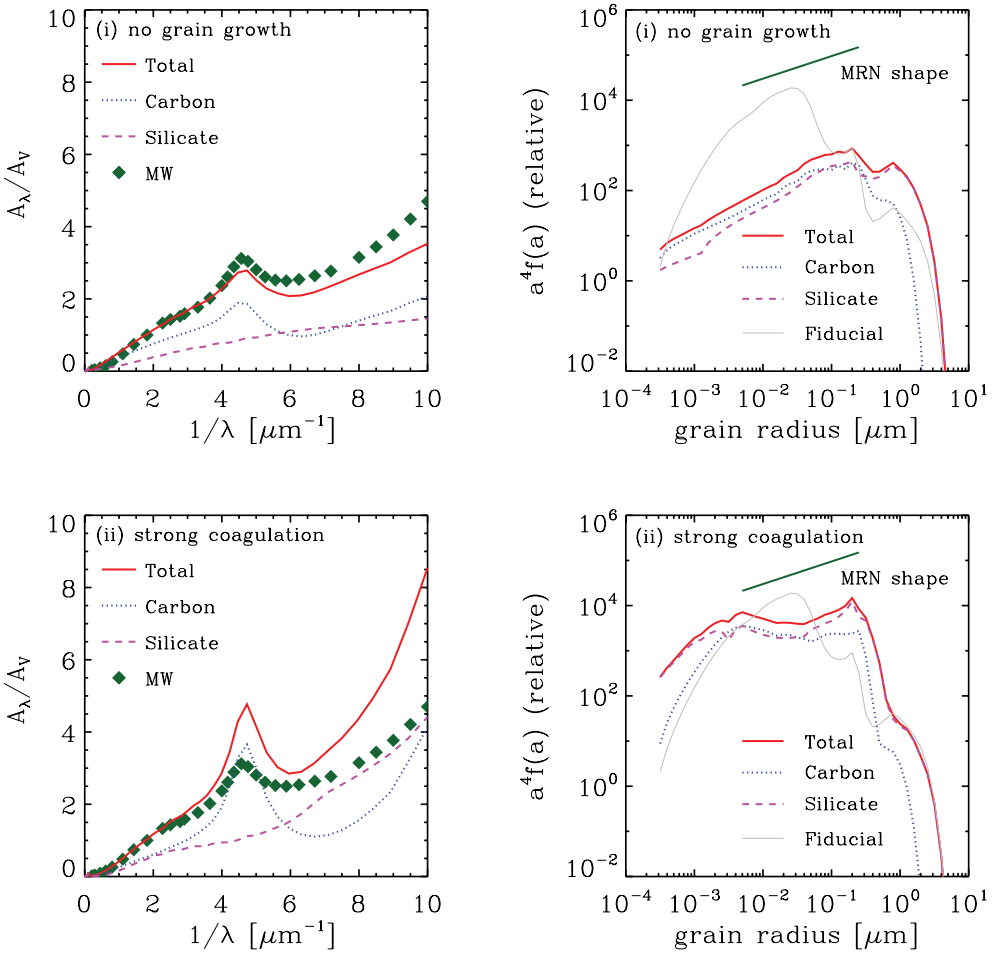

Figure 8. Extinction curves (left panels) and grain-size distributions (right panels) at galactic age 10 Gyr for total grains (solid line), carbon dust (dotted line) and silicate dust (dashed line). From top to bottom, the two panels represent the cases (i) without grain growth, and (ii) without a coagulation threshold velocity. For reference, we have plotted the results of the grain-size distribution using the same parameters as in Section 3.5 (thin solid line), and the MW extinction curve (filled diamonds; Whittet 2003). We adopt $\tau_{SF} = 5$ Gyr and $\eta_{WNM} = \eta_{CNM} = 0.5$.

the evolution of the total dust mass in galaxies, it is hard to reproduce the total dust mass of the Milky Way, as has been pointed out by, for example, Zhukovska et al. (2008), Draine (2009a), Inoue (2011) and Asano et al. (2013a). For example, Inoue (2011) showed that in the case without grain growth, the total dust amount in a galaxy is about 10 times lower than that in the Milky Way, even if dust grains are not destroyed by SN shocks. Thus, with this scenario we can obtain an extinction curve similar to that of the Milky Way, but we have difficulty in reproducing the total dust mass.

Next, we discuss the extinction curve for the case of strong coagulation (bottom panels). We observe that the extinction curve has a slightly larger bump and a steeper UV slope than the MW extinction curve, as the abundance of small grains ($a < 0.01$ μm) is slightly enhanced compared with the MRN size distribution. However, we find that the bump in the grain-size distribution can disappear. In this model, we remove the coagulation threshold, so the bump in the grain-size distribution can shift towards larger sizes than in the fiducial case. When the radius of grains reaches ∼0.2 μm, the grains are shattered effectively, and consequently the bump vanishes. Furthermore, owing to the supply of large grains by strong coagulation, shattering is induced, and, as a result, small grains are supplied. Hence, the number of small grains is larger than in the fiducial case. With such an interplay, the size distribution is expected to approach the power-law size distribution with a power index −3.5 (Tanaka et al. 1996; Kobayashi et al. 2010). Consequently, the extinction curve is nearer to the MW extinction curve than the cases in Section 3. In addition, unlike case (i), case (ii) may naturally account for the evolutions of the total dust mass, grain-size distribution and extinction curve in a galaxy at the same time. Note that power-law-like grain-size distributions can also reproduce the LMC and SMC extinction curves (Pei 1992). Thus, we conclude that the strong interplay of shattering and coagulation is important in reproducing the extinction curves observed in nearby galaxies.

4.2 Other possible grain species

As mentioned in Section 1, we do not consider PAHs in this work. PAHs are important in reproducing the SEDs at near- and mid-infrared wavelengths in galaxies (e.g. Li & Draine 2001), and they may contribute to the 2175-Å bump in the MW extinction curve (e.g. Weingartner & Draine 2001). However, what kinds of grains dominate the bump at 2175 Å is still a matter of debate (e.g. Draine & Malhotra 1993; Li & Draine 2001; Draine 2003). Furthermore, although carbon-rich AGB stars or shattering processes in grain–grain collisions are considered as possible sources of PAHs (e.g.

Latter 1991; Jones et al. 1996; Seok, Hirashita & Asano 2014), the main formation mechanism of PAHs is still controversial.

We do not consider other carbonaceous dust, such as glassy carbon or amorphous carbon. Nozawa & Fukugita (2013) discussed the effect of these species on extinction curves, and showed that they make the bump at 2175 Å small. This means that the 2175-Å bump that we calculated may be overestimated. Recently, Jones et al. (2013) constructed a dust model considering hydrogenated amorphous carbon without graphite, and the model reproduced the extinction curve, IR extinction, IR–mm dust emission, and albedo of the Milky Way. In fact, their best-fitting model also depends on the dust properties adopted. However, the trend that the small carbonaceous grains produce the 2175-Å bump and that large grains are responsible for flat extinction does not change. Thus, the evolutionary trend of the shape of extinction curves would not change significantly even if species other than graphite were adopted as representative carbonaceous species.

In this paper, we consider astronomical silicate as one of the main dust species. However, many observations have suggested that other species of cosmic silicate may exist as iron-poor ones such as enstatite ($MgSiO_3$) and forsterite (Mg_2SiO_4) (e.g. Draine 2003). In addition, many of the iron atoms are likely to be locked up in pure Fe grains (Draine 2009b) and other Fe-bearing grains such as magnetite (Fe_3O_4) and iron sulfide (FeS) (e.g. Cowie & Songaila 1985). Recently, Nozawa & Fukugita (2013) showed that the extinction curve produced by Fe or Fe_3O_4 or FeS grains in addition to the combination of graphite and Mg_2SiO_4 is similar to that led by the combination of graphite and astronomical silicate, as long as most of the Mg, Si, and Fe atoms are locked up in these grains. This indicates that astronomical silicate and the combination of other dust species have similar optical properties to each other. Thus, even if we were to consider other species of silicate grains, it is unlikely that this would significantly modify the discrepancy between the modelled and MW extinction curves.

4.3 Remarks on extinction in high-z galaxies

In Section 4.1, we compared our models with the MW extinction curve, and investigated the important physics that reproduces the MW extinction curve. Here, we consider the implications of our results for observed extinction curves in high-z galaxies.

The extinction curves in high-z galaxies have recently been explored by many authors (e.g. Maiolino et al. 2004; Gallerani et al. 2010; Hjorth et al. 2013). Indeed, from observations, Gallerani et al. (2010) showed that the extinction curves in high-z ($z > 4$) quasi-stellar objects (QSOs) tend to be flatter than those in nearby galaxies. In addition, these flat extinction curves in high-z galaxies are thought to be dominated by dust grains ejected by SNe II whose lifetimes are short (typically 10^{6-7} yr) (e.g. Maiolino et al. 2004; Hirashita et al. 2008). Our result, that the extinction curves in the early stage of galaxy evolution are relatively flat, is probably consistent with their results, although our extinction curves may be too flat. However, there is a suggestion that the large quantities of dust in dusty QSOs in the high-z Universe are regulated by grain growth (e.g. Michałowski et al. 2010; Kuo & Hirashita 2012). This claim is strengthened by the fact that these dusty QSOs in the high-z Universe have metallicity $Z > Z_\odot$ (e.g. Juarez et al. 2009). As shown by our calculations, once grain growth occurs, the extinction curve changes significantly. Thus, as investigated in Section 4.1, strong coagulation may be worth considering also for high-z QSOs. However, we should note that QSOs with steep extinction curves may be missing from the samples that have been observed by other authors because of the strong UV (optical in the observer's frame) extinction.

The rest-UV SEDs in high-z galaxies ($z \gtrsim 4$) have been investigated by a number of authors (e.g. Bouwens et al. 2009; González et al. 2012). In particular, it is reported that UV colours in these galaxies become bluer with increasing redshift (e.g. Bouwens et al. 2009). This fact is generally interpreted as reflecting low dust amounts in galaxies. However, the relation between extinction and UV colour depends on the extinction curve (Wilkins et al. 2013). In particular, the blue colour may be explained with a flat extinction curve as shown by our results in the early stage of galaxy evolution. Thus, there may be a significant amount of dust even in high-z galaxies with blue colours, which implies that the intrinsic luminosity may be underestimated.

The strong 2175-Å feature in star-forming galaxies at $1 < z < 2.5$ (the age of the Universe is ∼3–6 Gyr in a ΛCDM cosmological model with $\Omega_\Lambda = 0.7$, $\Omega_\mathrm{M} = 0.3$ and $H_0 = 70\,\mathrm{km\,s^{-1}\,Mpc^{-1}}$) is reported by Noll et al. (2007). They found robust evidence of the 2175-Å bump in one-third of their sample. The existence of the 2175-Å bump in galaxies at these redshifts supports our results that the bump becomes strong in galaxies at $t \sim \tau_\mathrm{shat} \sim 1\,(\tau_\mathrm{SF}/\mathrm{Gyr})^{1/2}$ Gyr with $\tau_\mathrm{SF} \lesssim 10$ Gyr. Thus, shattering and grain growth may be effective in these galaxies, and the variation of the extinction curve can be explained by the difference of the galactic age and the star formation time-scale.

5 CONCLUSION

We investigated the evolution of extinction curves in galaxies based on the evolution model of grain-size distribution (A13). We took into account various dust processes: dust formation by SNe II and AGB stars, dust reduction through astration, dust destruction by SN shocks in the ISM, grain growth in the CNM, and grain–grain collisions (shattering and coagulation) in the WNM and CNM.

We found that the extinction curve is flat in the early stage of galaxy evolution because of the large grains ($a \gtrsim 0.1$ μm) produced by stars. As galactic evolution proceeds, shattering becomes effective, and the number of small grains increases. Later, these small grains grow owing to grain growth, forming a bump at $a \sim 10^{-3}$–10^{-2} μm in the grain-size distribution. Because the relatively small grains are dominant in grain-size distribution, the extinction curve has a large bump at $1/\lambda \sim 4.5\,\mu\mathrm{m}^{-1}$ and a steep UV slope. The time-scale on which dust processes in the ISM (grain growth, shattering and coagulation) begin to control the grain-size distribution is estimated as $t \sim 1(\tau_\mathrm{SF}/\mathrm{Gyr})^{1/2}$ Gyr. After coagulation occurs effectively, the extinction curves become flatter but still tend to be steeper than the MW extinction curve. We also found that for reproduction of the MW extinction curve, it may be important to consider a larger contribution of coagulation than that which we have assumed. This means that the strong interplay between shattering and coagulation induced by strong coagulation could be essential to reproduce the MW extinction curve. We conclude that the extinction curves in galaxies drastically change with galactic age because of the evolution of the grain-size distribution.

ACKNOWLEDGEMENTS

We thank the anonymous referee for her/his helpful comments, which improved the quality and clarity of this paper. We are grateful to Takashi Kozasa, Anthony P. Jones, Daisuke Yamasawa and Asao Habe for fruitful discussions. We thank H. Kobayashi for helpful discussions on the process of the grain–grain collisions and the

evolution of the grain-size distribution. RSA was supported by a Grant-in-Aid for JSPS Research under Grant No. 23-5514. TTT was supported by the Strategic Young Researcher Overseas Visits Program for Accelerating Brain Circulation No. R2405 and the Grant-in-Aid for Scientific Research Fund (20740105, 23340046) commissioned by the MEXT. HH is supported by NSC grant 102-2119-M-001-006-MY3. TN was supported by the World Premier International Research Center Initiative (WPI Initiative), MEXT, Japan, and by the Grant-in-Aid for Scientific Research of the JSPS (22684004, 23224004).

REFERENCES

Asano R. S., Takeuchi T. T., Hirashita H., Inoue A. K., 2013a, Earth Planets and Space, 65, 213
Asano R. S., Takeuchi T. T., Hirashita H., Nozawa T., 2013b, MNRAS, 432, 637 (A13)
Barbaro G., Mazzei P., Morbidelli L., Patriarchi P., Perinotto M., 2001, A&A, 365, 157
Bianchi S., Schneider R., 2007, MNRAS, 378, 973
Bouwens R. J. et al., 2009, ApJ, 705, 936
Buat V., Donas J., Milliard B., Xu C., 1999, A&A, 352, 371
Cardelli J. A., Clayton G. C., Mathis J. S., 1989, ApJ, 345, 245
Cazaux S., Spaans M., 2009, A&A, 496, 365
Cazaux S., Tielens A. G. G. M., 2004, ApJ, 604, 222
Chokshi A., Tielens A. G. G. M., Hollenbach D., 1993, ApJ, 407, 806
Cowie L. L., Songaila A., 1986, ARA&A, 24, 499
Di Criscienzo M. et al., 2013, MNRAS, 433, 313
Draine B. T., 2003, ARA&A, 41, 241
Draine B. T., 2009a, in Henning Th., Grün E., Steinacker J., eds, ASP Conf. Ser. Vol. 414, Cosmic Dust – Near and Far. Astron. Soc. Pac., San Francisco, p. 453
Draine B. T., 2009b, Space Sci. Rev., 143, 333
Draine B. T., Lee H. M., 1984, ApJ, 285, 89
Draine B. T., Malhotra S., 1993, ApJ, 414, 632
Fitzpatrick E. L., Massa D., 2007, ApJ, 663, 320
Gallerani S. et al., 2010, A&A, 523, 85
González V., Bouwens R. J., Labbé I., Illingworth G., Oesch P., Franx M., Magee D., 2012, ApJ, 755, 148
Hirashita H., 2012, MNRAS, 422, 1263
Hirashita H., Ferrara A., 2002, MNRAS, 337, 921
Hirashita H., Kuo T.-M., 2011, MNRAS, 416, 1340
Hirashita H., Li Z.-Y., 2013, MNRAS, 434, L70
Hirashita H., Yan H., 2009, MNRAS, 394, 1061
Hirashita H., Nozawa T., Takeuchi T. T., Kozasa T., 2008, MNRAS, 384, 1725
Hirashita H., Nozawa T., Yan H., Kozasa T., 2010, MNRAS, 404, 1448
Hjorth J., Vreeswijk P. M., Gall C., Watson D., 2013, ApJ, 768, 173
Inoue A. K., 2011, Earth Planets and Space, 63, 1
Jones A. P., Tielens A. G. G. M., Hollenbach D. J., 1996, ApJ, 469, 740
Jones A. P., Fanciullo L., Köhler M., Verstraete L., Guillet V., Bocchio M., Ysard N., 2013, A&A, 558, A62
Juarez Y., Maiolino R., Mujica R., Pedani M., Marinoni S., Nagao T., Marconi A., Oliva E., 2009, A&A, 494, L25
Kobayashi H., Tanaka H., Krivov A. V., Inaba S., 2010, Icarus, 209, 836
Kobayashi M. A. R., Inoue Y., Inoue A. K., 2013, ApJ, 763, 3
Krühler T. et al., 2013, A&A, 557, 18
Kuo T.-M., Hirashita H., 2012, MNRAS, 424, L34
Latter W. B., 1991, ApJ, 377, 187
Li A., Draine B. T., 2001, ApJ, 554, 778
Liang S. L., Li A., 2009, ApJ, 690, L56
Liffman K., Clayton D. D., 1989, ApJ, 340, 853
Maiolino R., Schneider R., Oliva E., Bianchi S., Ferrara A., Mannucci F., Pedani M., Roca Sogorb M., 2004, Nature, 431, 533
Mathis J. S., Rumpl W., Nordsieck K. H., 1977, ApJ, 217, 425 (MRN)
Matsuoka Y., Oyabu S., Tsuzuki Y., Kawara K., Yoshii Y., 2005, PASJ, 57, 563
Michałowski M. J., Murphy E. J., Hjorth J., Watson D., Gall C., Dunlop J. S., 2010, A&A, 522, A15
Noll S., Pierini D., Pannella M., Savaglio S., 2007, A&A, 472, 455
Nozawa T., Fukugita M., 2013, ApJ, 770, 27
Nozawa T., Kozasa T., Habe A., 2006, ApJ, 648, 435
Nozawa T., Kozasa T., Habe A., Dwek E., Umeda H., Tominaga N., Maeda K., Nomoto K., 2007, ApJ, 666, 955
O'Donnell J. E., Mathis J. S., 1997, ApJ, 479, 806
Omukai K., Tsuribe T., Schneider R., Ferrara A., 2005, ApJ, 626, 6270
Ormel C. W., Paszun D., Dominik C., Tielens A. G. G. M., 2009, A&A, 502, 845
Ossenkopf V., 1993, A&A, 280, 617
Pei Y. C., 1992, ApJ, 395, 130
Schneider R., Omukai K., Inoue A. K., Ferrara A., 2006, MNRAS, 369, 1437
Seok J. Y., Hirashita H., Asano R. S., 2014, MNRAS, in press
Sofia U. J., Meyer D. M., 2001, ApJ, 554, L221
Takagi T., Vansevičius V., Arimoto N., 2003, PASJ, 55, 385
Tanaka H., Inaba S., Nakazawa K., 1996, Icarus, 123, 450
Todini P., Ferara A., 2001, MNRAS, 325, 726
Valiante R., Schneider R., Bianchi S., Andersen A. C., 2009, MNRAS, 397, 1661
Ventura P. et al., 2012a, MNRAS, 420, 1442
Ventura P. et al., 2012b, MNRAS, 424, 2345
Weingartner J. C., Draine B. T., 2001, ApJ, 548, 296
Whittet D. C. B., 2003, Dust in the Galactic Environment, 2nd edn. IoP Publishing, Bristol, p. 76
Wilkins S. M., Bunker A., Coulton W., Croft R., Matteo T. D., Khandai N., Feng Y., 2013, MNRAS, 430, 2885
Winters J. M., Fleischer A. J., Le Bertre T., Sedlmayr E., 1997, A&A, 326, 305
Wolfire M. G., McKee C. F., Hollenbach D., Tielens A. G. G. M., 2003, ApJ, 587, 278
Yamasawa D., Habe A., Kozasa T., Nozawa T., Hirashita H., Umeda H., Nomoto K., 2011, ApJ, 735, 44
Yan H., Lazarian A., Draine B. T., 2004, ApJ, 616, 895
Yasuda Y., Kozasa T., 2012, ApJ, 745, 159
Zhukovska S., Gail H. P., Trieloff M., 2008, A&A, 479, 453

This paper has been typeset from a TEX/LATEX file prepared by the author.